www.czasopisma.pan.pl PAN POLSKA AKADEMIA NAUK www.journals.pan.pl

Arch. Metall. Mater. **62** (2017), 1, 235-239

DOI: 10.1515/amm-2017-0035

J. PIETRASZEK*#, A. SZCZOTOK**, N. RADEK***

THE FIXED-EFFECTS ANALYSIS OF THE RELATION BETWEEN SDAS AND CARBIDES FOR THE AIRFOIL BLADE TRACES

The primary objective was to test a usefulness of the specific fixed-effect model for the analysis of quantitative relationships gathered from the image analysis of the material microstructures. The dataset was obtained from the investigation of turbine blades made from superalloy IN713C. The analysis based on the general linear model resulted in informative plots revealing mutual relationships between secondary dendrite arm spacing and the mean plane section area of carbides in the material. Directions for further research also were obtained.

Keywords: microstructure, SDAS, carbide, IN 713C, superalloy

1. Introduction

Turbine blades in aero-engine and land-based power generation gas turbines are complex components manufactured to precise geometric, structural and mechanical property tolerances [1]. The investment casting process is extensively used today to produce "net shape" structural parts for aircraft engines [2]. Solidification defects, and especially microporosity, are still the main reason for the high rejection rate of the castings [3]. That is why a knowledge about the growth of the initial dendritic microstructure during solidification based on experimental and theoretical studies is required to control the formation of solidification defects. Numerous studies of secondary dendrite arm spacing (SDAS) and dendrite growth in cast Ni-based superalloys have been carried out in order to optimize casting and microstructure parameters [4-6].

2. Materials and methods

The three airfoil blade castings from IN713C superalloy coming from one pattern assembly cast at the laboratory scale (Fig. 1) were investigated using light microscopy (LM) and scanning electron microscopy (SEM) to check repeatability of the microstructure depending on a various location in the pattern assembly (Fig. 2). The main goal of the studies was to evaluate an impact of these locations and the solidification conditions on SDAS and the mean plane section area of carbides in the material. The fixed-effects models were used as the typical approach to analyze such cases. The procedure and results are presented in this paper.

Fig. 1. The pattern assembly with 20 airfoil blade castings

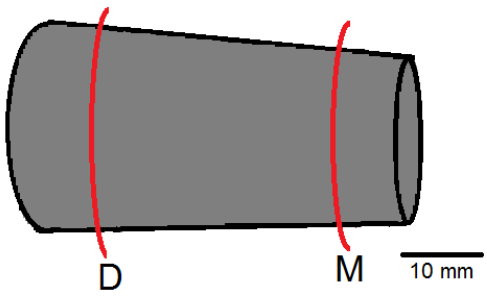

Fig. 2. The scheme of an airfoil blade and a position of cross-sections

* CRACOW UNIVERSITY OF TECHNOLOGY, FACULTY OF MECHANICAL ENGINEERING, DEPARTMENT OF SOFTWARE ENGINEERING AND APPLIED STATISTICS, AL. JANA PAWLA II 37, 31-864 KRAKOW, POLAND
** SILESIAN UNIVERSITY OF TECHNOLOGY, FACULTY OF MATERIALS ENGINEERING AND METALLURGY, INSTITUTE OF MATERIALS SCIENCE, 8 KRASINSKIEGO STR., 40-019 KATOWICE, POLAND
*** TECHNICAL UNIVERSITY OF KIELCE, CENTRE FOR LASER TECHNOLOGIES OF METALS, AL. 1000-LECIA PANSTWA POLSKIEGO 7, 25-314 KIELCE, POLAND
# Corresponding author: pmpietra@gmail.com

Airfoil Blades. Three airfoil blades selected randomly from the pattern assembly were cut to obtain two cross-sections from the each airfoil blade in the way presented in Fig. 2. The microstructure of the casting was evaluated through standard metallographic techniques, including sectioning, grinding, polishing, and etching followed by optical and scanning electron microscopy. The cross-sections were included and prepared according to the scheme worked out for Ni-based superalloys [7]. The secondary dendrite arm spacings were measured from the LM photographs (GX-51 Olympus LM). The SDAS was measured using a line intercept method. The mean plane section area of carbides was evaluated on the basis of SEM images (Hitachi S-4200 SEM).

The etched surface of the metallographic specimens were observed by LM, then SEM and automatically analyzed by the image analysis program [8]. The dataset contains two elements: SDAS and the size of carbides. The obtained raw data should be compared to find if the different conditions differentiate the properties between blades in two different geometrical locations.

Microstructural studies. The selected examples of carbide detection were presented in the Fig. 3 and Fig. 4.

The selected examples of dendritic structure in the investigated cross-sections were presented in the Fig. 5.

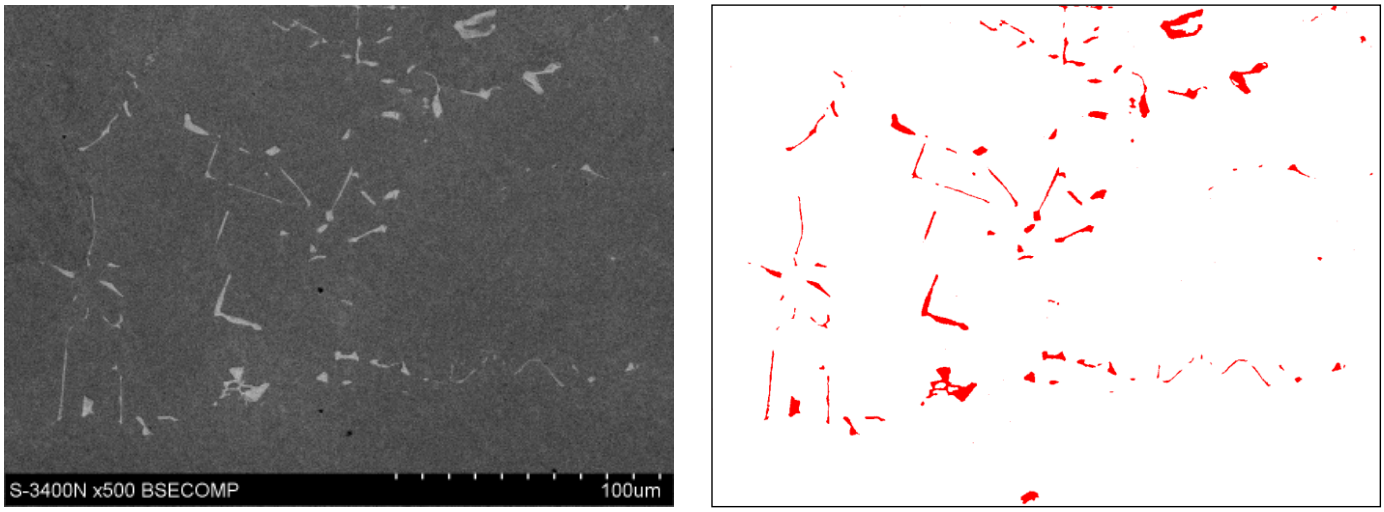

Fig. 3. The carbides detected in the selected image of B2D cross-section

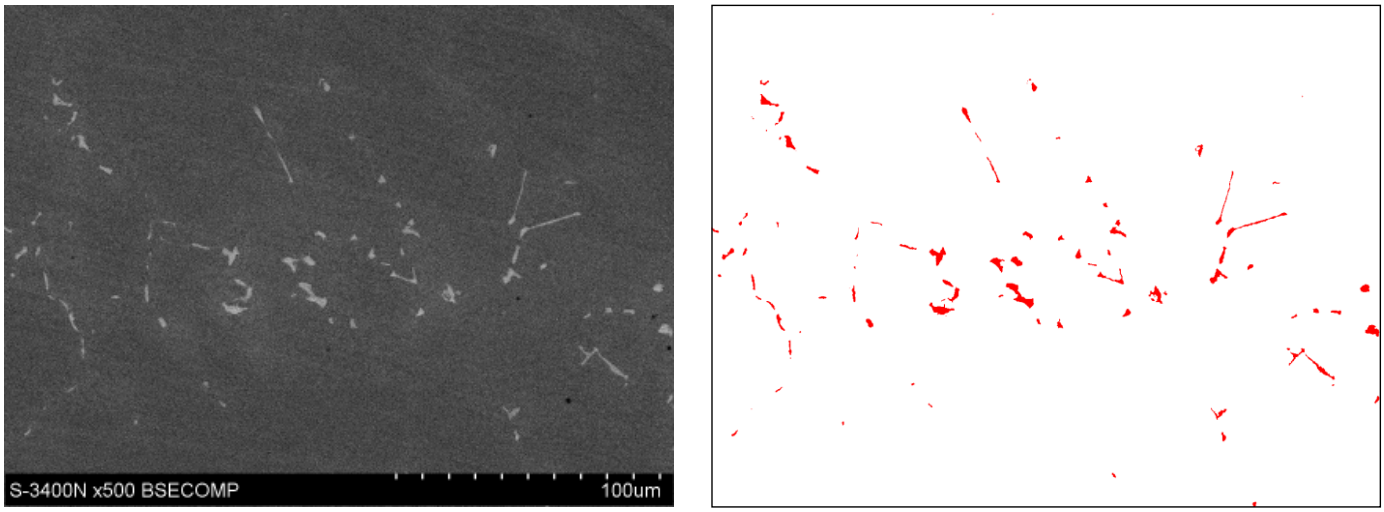

Fig. 4. The carbides detected in the selected image of B2M cross-section

Fixed Effects Model. The fixed-effects model is a typical approach if independent variables (factors) are qualitative labels instead of quantitative values [9]. The model is constructed from some additive terms [10]: average response μ, vectors of main (linear) effects dependent on the single factor (blade id or trace id) and a matrix of two-way interaction dependent simultaneously on the both factors. This analysis depends on the assignment of the residuum normality however it is possible to conduct such computations without this requirement [11] but with significantly much greater computational cost.

In the considered case, the fixed-effects model has the following formula:

$$g_{ij} = \mu + A_i + B_j + C_{ij} \tag{1}$$

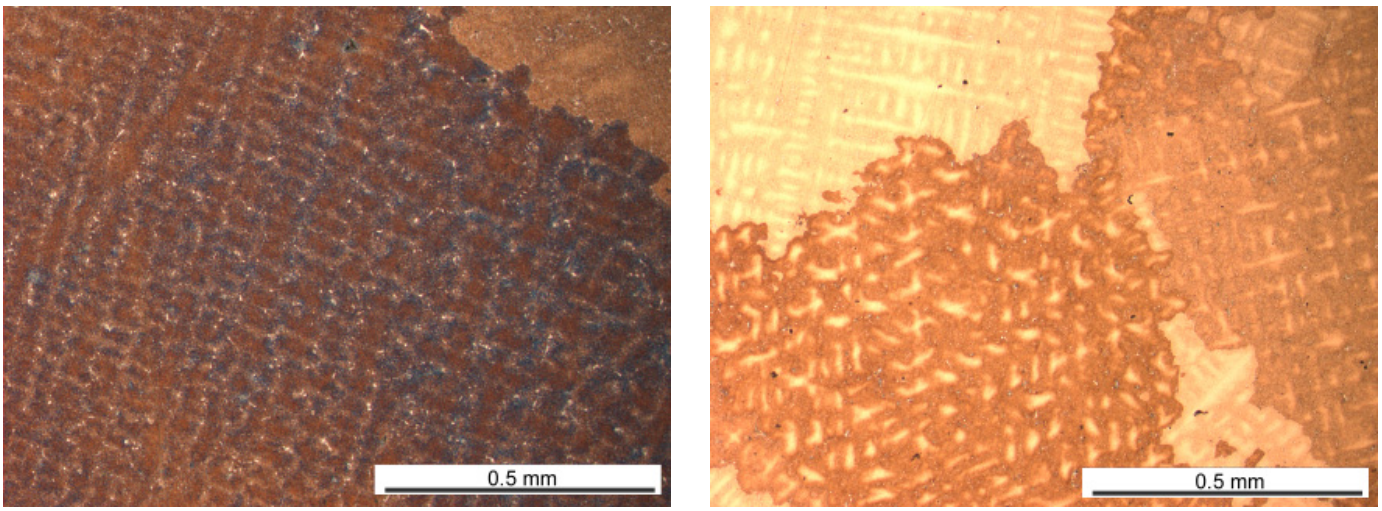

Fig. 5. The dendritic structure in the selected D (left B1D) and M (right B1M) cross-sections

where:

μ – average response,
A_i – main (linear) effect of blade id,
i – enumerator of a blade id i.e. B1, B2, B3,
B_j – main (linear effect) of trace id,
j – enumerator of a trace id i.e. D or M,
C_{ij} – two-way interaction of blade and trace ids.

Due to the lack of redundant data, it is not possible to provide a pure error estimation and full ANOVA analysis. The only possible data analysis is to identify models for SDAS and carbide content and then to compare means and interaction effects and to construct marginal means plot and interaction plot.

3. Results

Three air-foil blades were manufactured at three different conditions labelled as B1, B2 and B3. Each blade were cut at two positions forming traces: D and M. The data are presented in Table 1.

TABLE 1

SDAS and carbide content observed for different blades and traces (SDAS – mean, C – median of mean plane section area of carbides)

Trace	Blade					
	B1		B2		B3	
	SDAS [µm]	C [µm^2]	SDAS [µm]	C [µm^2]	SDAS [µm]	C [µm^2]
D	43.7	2.78	55.3	2.16	48.5	1.92
M	37.4	1.22	39.0	1.18	38.6	0.92

The identification of the simple fixed-effect model based only on linear effects led – in both cases SDAS and C – to completely insignificant results due to the very large error term. It was caused by an interaction. However, the enhanced model – linear effects with two-way interaction – required to scarify the error term due to the lack of redundant data. The model identified for SDAS is presented in Table 2, while the model identified for C is presented in Table 3.

TABLE 2

The fixed-effects model with linear effects and two-way interaction identified for mean of SDAS and two factors: blade id and trace id

Effect	Level	Coefficient	Effect	Level	Coefficient
constant	—	43.750	Blade ×trace	B1×D	–2.267
blade	B1	–3.200		B2×D	2.733
	B2	3.400		B3×D	–0.466
	B3	–0.200		B1×M	2.267
trace	D	5.417		B2×M	–2.733
	M	–5.417		B3×M	0.466

TABLE 3

The fixed-effects model with linear effects and two-way interaction identified for median of carbides C and two factors: blade id and trace id

Effect	Level	Coefficient	Effect	Level	Coefficient
constant	—	1.697	Blade ×trace	B1×D	0.1889
blade	B1	0.3067		B2×D	–0.0988
	B2	–0.0280		B3×D	–0.0901
	B3	–0.2787		B1×M	–0.1889
trace	D	0.5916		B2×M	0.0988
	M	–0.5916		B3×M	0.0901

The main effects plot and interaction plot for SDAS are presented in (Fig. 6) and (Fig. 7), respectively.

The main effects plot and interaction plot for carbides are presented in (Fig. 8) and (Fig. 9), respectively.

The simultaneous plot of mean of SDAS against median of carbides C (Fig. 10) reveals some minor monotonic correlation between both properties except of B1D case which drastically differs from the growing trend.

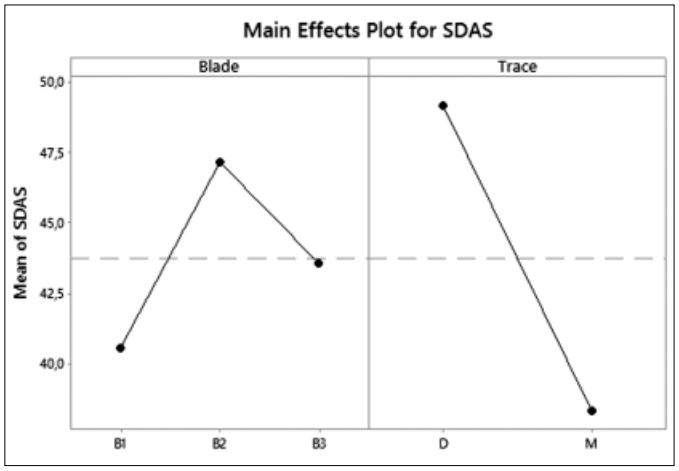

Fig. 6. The main effects plot for mean of SDAS.Blades: B1, B2, B3. Traces: D and M

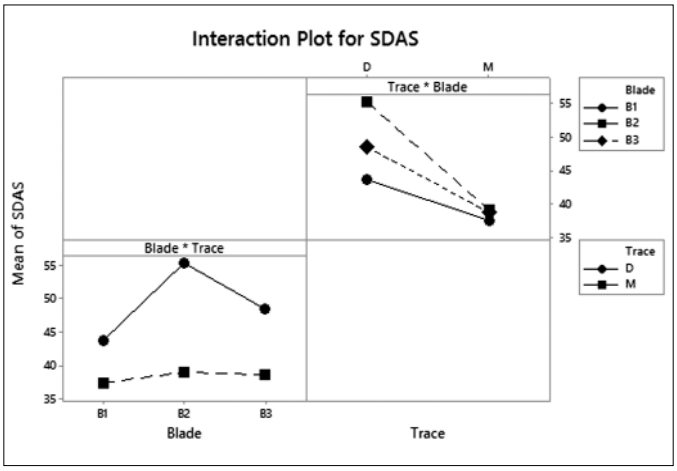

Fig. 7. The interaction plot for mean of SDAS

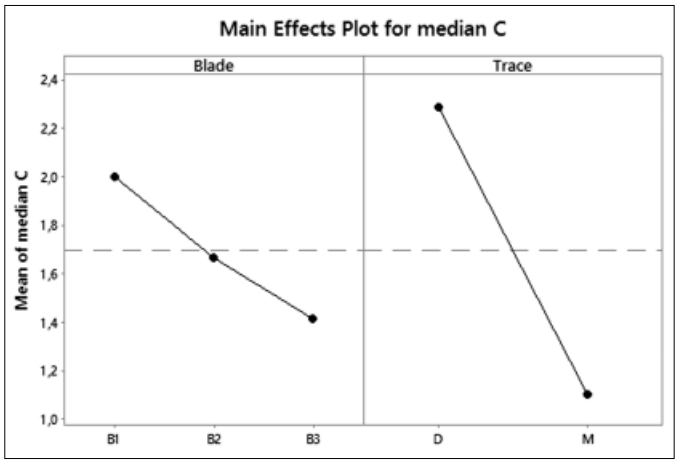

Fig. 8. The main effects plot for median of C.Blades B1, B2, B3. Traces D and M

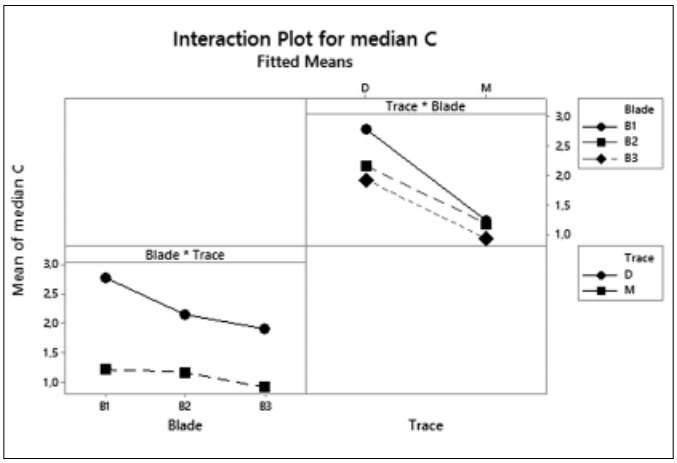

Fig. 9. The interaction plot for median of C

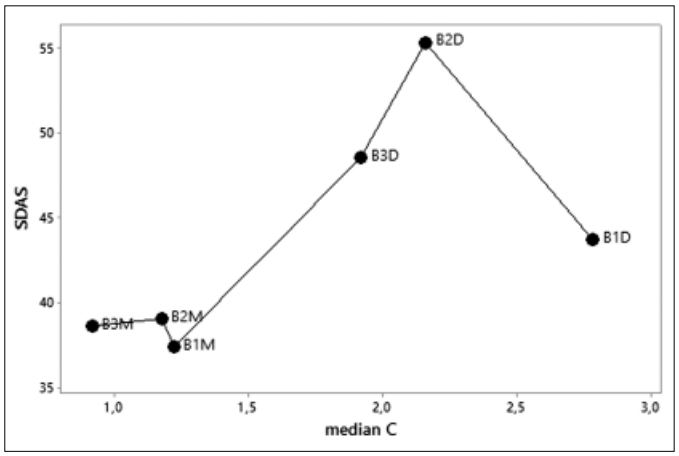

Fig. 10. The plot of mean of SDAS against median of

4. Discussion

Statistically, the SDAS model revealed strong interaction between blade id and trace id, while the C model showed rather weak interaction. The SDAS weakly monotonically correlates (in the sense of Spearman's correlation) to C median, however one case (B1D) drastically differs from such scheme.

Technologically, it means that SDAS differences between traces strongly depends on manufacturing treatments and cannot be treated as constant bias. In contrast, the C differences between traces may be practically treated as constant and mutually equal – interaction is weak and only slightly changes that differences. The weak correlation between SDAS and carbide's content means that practically may be predicted: lower carbides-lower SDAS and greater carbides-greater SDAS with one exception: B1D case which differs from such monotonic relationship. It's worth to make further investigation on that particular case to eliminate such dissimilarity (if it is artifact) or to reveal some hidden factor or significant phenomenon making such difference.

5. Conclusions

The mean size of the carbides from the cross-sections of the investigated castings is greater in cross-sections D than cross-

sections B. This may be due to a slower time of solidification in location D of the airfoil blade than in B.

The results affirmed that the crystallization conditions (variable casting wall thickness, location of the feeding sprue) influence the microstructure, especially the SDAS and mean plane section area of carbides occurring in the material.

The presented Research methodology can be applied to optimize the industrial production of aircraft components or – after minor modification – in bioceramic components production and analysis [12,13]. The further investigation on data analysis will be conducted involving specific non-parametric methods for the analysis of multidimensional sparse data [14-20], even with a multiphysics approach [21] and the fuzzy statistics [22].

Acknowledgements

Financial support from the Structural Funds in the Operational Programme – Innovative Economy (IE OP) financed from the European Regional Development Fund – Project No POIG.0101.02-00-015/08 is gratefully acknowledged.

REFERENCES

[1] D.C. Power, Platinum Metals Rev. **39**, 117-126 (1995).
[2] G. Sjoberg, in: E. Ott, J. Groh, A. Banik, I. Dempster, T. Gabb, R. Helmink, X. Liu, A. Mitchell, G.P. Sjoberg, A. Wusatowska-Sarnek (Eds.), 7th International Symposium on Superalloy 718 & Derivatives, October 10-13, 2010, Pittsburgh, Pennsylvania 117-130, 2010.
[3] M.D. Kang, H.Y. Gao, J. Wang, L.S.B. Ling, B.D. Sun, Materials **6**, 1789-180 (2013).
[4] V. Kavoosi, S.M. Abbasi, S.M.G. Mirsaed, M. Mostafaei, J. Alloy Compd. **680**, 291-300 (2016).
[5] L. Liu, T.W. Huang, Y.H. Xiong, A.M. Yang, Z.L. Zhao, R. Zhang, J.S. Li, Mat Sci Eng a-Struct **394**, 1-8 (2005).
[6] Y. Zhuhuan, L. Lin, Z. Xinbao, China Foundry **7**, 217-223 (2010).
[7] Buehler SUM-MET: The Science Behind Materials Preparation. Buehler, USA, 2004.
[8] A. Gądek, S. Kuciel, L. Wojnar, W. Dziadur, Polimery **51**, 206-211 (2006).
[9] D.C. Montgomery, Design of Experiments. John Wiley and Sons, Hoboken, 2003.
[10] L. Davies, U. Gather, in: J.E. Gentle, W.K. Hardle (Eds.), Handbook of Computational Statistics, Springer-Verlag, Berlin-Heidelberg 742-745, 2012.
[11] J. Pietraszek, A. Gądek-Moszczak, Solid State Phenom. **197**, 162-167 (2013).
[12] A. Dudek, C. Kolan, Solid State Phenom. **165**, 25-30 (2010).
[13] A. Dudek, R. Włodarczyk, Solid State Phenom. **165**, 31-36 (2010).
[14] A. Gadek-Moszczak, L. Wojnar, ECS10: The10th European Congress of Stereology and Image Analysis, 2009, 453-458.
[15] E. Skrzypczak-Pietraszek, A. Hensel, Pharmazie **55**, 2000, 768-771.
[16] R. Skulski, P. Wawrzala, J. Korzekwa, M. Szymonik, Arch. Metall. Mater. **54**, 2009, 935-941.
[17] J. Pietraszek, 6th International Conference on Neural Networks and Soft Computing, 2003, 250-255.
[18] J. Korzekwa, R. Tenne, W. Skoneczny, G. Dercz, Phys. Status Solidi A **210**, 2013, 2292-2297.
[19] L. Skrzypczak, E. Skrzypczak-Pietraszek, E. Lamer-Zarawska, B. Hojden, Acta Soc. Bot. Pol. **63**, 1994, 173-177.
[20] N. Radek, A. Sladek, J. Broncek, I. Bilska, A. Szczotok, Adv. Mater. Res. **874**, 2014, 101-106.
[21] T. Styrylska, J. Pietraszek, Z. Angew. Math. Mech. **72**, 1992, T537-T539.
[22] J. Pietraszek, M. Kolomycki, A. Szczotok, R. Dwornicka, 8th International Conference on Computational Collective Intelligence (ICCCI), 2016, 260-268.